



Ultrafine copper decorated polypyrrole nanotube electrode for nitrite detection

Yuqing Shen¹ · Guodong Zhu¹ · Jianmao Yang² · Jianyun Liu¹

Received: 3 February 2018 / Revised: 22 April 2018 / Accepted: 23 April 2018 / Published online: 5 May 2018
© Springer-Verlag GmbH Germany, part of Springer Nature 2018

Abstract

In this report, a nitrite electrochemical sensor was developed by electrochemical deposition of copper nanoparticles on the polypyrrole nanotubes (PPy-Cu). The PPy nanotubes were synthesized via pyrrole polymerization on electrospun polystyrene nanofibers (PS) with the diameter of 150 nm, followed by PS removal. The prepared nanotubes were characterized using Fourier transform infrared spectroscopy (FT-IR) and scanning electron microscopy (SEM). Ultrafine Cu nanoparticles with the size of 4.2 ± 1.2 nm were uniformly deposited on PPy tubes by electrolysis. The existence of zero valence Cu particles was demonstrated by transmission electron microscopy (TEM) and X-ray photo spectroscopy (XPS). The electrochemical behaviors of the PPy and PPy-Cu electrodes were investigated by cyclic voltammetry (CV). PPy enhances the deposition of Cu dramatically and facilitates the uniform distribution of the copper nanoparticles. The obtained PPy-Cu exhibits an excellent catalytic activity to the reduction of nitrite. The catalytic performance of the resultant PPy-Cu electrodes was optimized by varying the PPy morphology and Cu deposition amount. Using hydrodynamic current-time curves, the linear relationship was obtained, under the optimized conditions, in the range of 0.1 μ M to 1 mM with a limit of detection of 0.03 μ M ($S/N > 3$). The sensor presents good reproducibility and stability for nitrite determination.

Keywords Electrospinning · Polypyrrole nanotubes · Copper nanoparticle · Nitrite reduction

Introduction

Conducting polymers, due to the special physical and chemical properties, are becoming more and more attractive in a diversity of fields with the rapid development of electric industries and information technologies [1]. Conducting polymers include polyacetylene (PA) [2, 3], polyaniline (PANI) [4–6], polymelamine (PMel) [7, 8], polypyrrole (PPy) [9, 10], and polythiophene (PT) [9, 11]. Among these conducting

polymers, PPy, as one of the most popular candidates, finds widespread applications ranging across solar cell [10], electrochromic device [12], photodiode [13], supercapacitor [14, 15], and electrochemical sensor [16–18] due to the excellent features of high conductivity, high stability, good biocompatibility, facile fabrication, and low cost [17, 19]. Morphologically, various forms of PPy nanomaterials have been fabricated, including cauliflower nanospheres [10], nanowire [20, 21], and nanotubes [22]. Among these, three-dimensional nanotube has a high specific surface area and accessible active sites for ion transportation. Moreover, their inner and outer diameters as well as the aspect ratio of the tubes are tunable for different applications. This fabrication process and the form are controllable during synthesis typically by an electro-spinning technique.

Nano-structured PPy has often been used as a conducting matrix or support for deposition of metal nanoparticles because of its porous structure, excellent conductivity, and high specific surface area [17, 23]. Meanwhile, the metal agglomeration can be abated due to the interaction of pyrrolic N and metal [24, 25]. PPy-Pt [10, 16], PPy-Ag [21, 26, 27], and PPy-Au [28, 29] have been successfully fabricated for adsorption,

Electronic supplementary material The online version of this article (<https://doi.org/10.1007/s11581-018-2577-4>) contains supplementary material, which is available to authorized users.

✉ Jianyun Liu
jianyun.liu@dhu.edu.cn

¹ College of Environmental Science and Engineering, State Environmental Protection Engineering Center for Pollution Treatment and Control in Textile Industry, Donghua University, Shanghai 201620, People's Republic of China

² Research Center for Analysis & Measurement, Donghua University, Shanghai 201620, People's Republic of China

catalysis, energy storage, and sensing applications. Base metal copper nanoparticles possess unique catalytic activity in a variety of fields including chemical synthesis, sensor, and energy storage [30–32]. In addition, it has excellent advantages of good conductivity, strong redox property, low cost, and natural abundance, compared with the noble metals. The combination of Cu and PPy may achieve the synergetic effect for catalysis application. However, in the PPy/metal composite preparation, PPy was prepared mostly by electropolymerization [25, 33] or bulk synthesis [34, 35], which leads to dense and thick film, difficult for the even deposition of the highly dispersed metal particles. Three-dimensional PPy nanotube is supposed to provide huge surface area and a large quantity of active sites for the effective interaction of PPy and Cu, preventing the agglomeration of Cu. However, to our knowledge, the Cu nanoparticles decorated PPy nanotube composite has not been reported to date.

In this article, we present a PPy nanotube fabrication method using Py polymerization on an electrospun PS fiber followed by solvent etching. The morphology of PPy nanotubes can be tuned by Py concentration. By convenient one-step electrolysis, Cu nanoparticles are deposited on the PPy tubes. The influence of PPy structure on Cu deposition and the catalytic performance to nitrite reduction are investigated. The well-defined three-dimensional tubular structure facilitates the Cu deposition. In light of synergetic effect of PPy and Cu on the reduction of nitrite, the PPy-Cu electrode has been used as a sensitive sensor for nitrite determination. In addition, the drop-cast method is easy for batch fabrication and the obtained PPy-Cu electrode is very stable and reusable without loss of activity, showing a great potential for future sensing application.

Experiments

Reagents

Pyrrole (Py, $\geq 98\%$), polystyrene (PS, Mw = 280,000), and polyvinylidene fluoride (PVDF) were purchased from Sigma-Aldrich. Py was purified by reduced pressure distillation. *N,N*-Dimethylformamide (DMF), tetrahydrofuran (THF), and 1-methyl-pyrrolidone (NMP) were supplied by Lingfeng Reagent (Shanghai). All other chemicals (analytical grade) were obtained from Sinopharm Chemical Reagent Company and used as received. The ultrapure water (18.2 M Ω cm, 25 °C, Thermo Fisher Scientific) was used for aqueous solution preparation.

PS nanotube preparation

The PS nanofibers (about 150 nm in diameter) were prepared by electrospinning method analogous to that reported

previously [36]. The PS nanofibers were sulfonated in a concentrated sulfuric acid (98%) for 4 h at 40 °C to facilitate the growth of PPy. Following the cleaning of sulfonated fibers with ultrapure water, they were soaked in various concentrations of Py ethanol solution (0.2%, 0.4%, 0.6%, 0.8%, v/v) for 24 h to adsorb Py monomer onto the PS surface. The oxidation polymerization of Py occurred upon the addition of FeCl₃ solution to the above solution [n(FeCl₃):n(Py) = 1:1]. The polymerization reaction lasted for 24 h at 4 °C. Subsequently, the inner PS core of PS/PPy fiber was removed by THF wash. The final PPy nanotubes were obtained after ethanol and water wash followed by vacuum dry (50 °C) for 10 h. PPy tubes synthesized by 0.2%, 0.4%, 0.6%, and 0.8% Py were named as PPy(0.2), PPy(0.4), PPy(0.6), and PPy(0.8), respectively.

Preparation of PPy-Cu modified glassy carbon electrode

A glassy carbon electrode (GCE; $\varnothing = 3$ mm) was first polished successively with 1.0 and 0.3 μm Al₂O₃ slurries and then sonicated with a mixture of water and ethanol after each polishing. Subsequently, GCE was dried with high purity nitrogen to obtain a mirror-like surface. A suspension solution of PPy nanotubes was prepared by dispersing PPy nanotubes and PVDF solvent (PPy:PVDF = 8:1, weight ratio) in 10 mL NMP and sonicating for 10 min. The PPy nanotube-modified glassy carbon electrode (PPy/GCE) was obtained by drop coating 5 μL of the above suspension onto a clean GCE surface and dry under N₂ gas.

The deposition of copper nanoparticles on the PPy/GCE was performed by electrolysis at -0.7 V for 200 s in 0.1 M H₂SO₄ aqueous solution in the presence of 0.05 M CuSO₄ and 1 mM KCl. Following the thorough wash by water, the PPy-Cu modified glassy carbon electrode (PPy-Cu/GCE) was obtained.

The effective active surface areas of GCE, PPy/GCE, and PPy-Cu/GCE were calculated to be 0.11, 0.20, and 0.18 cm² by CV in 1 mM K₃[Fe(CN)₆] solution, based on the literature method [37]. The detailed calculation can be found in SI (Fig. S1). The slight decrease of surface area after Cu deposition is presumably due to the interaction of partial oxidized Cu ions in PPy-Cu with [Fe(CN)₆]³⁻ to form the deposit during CV scan [38].

Characterization method

Scanning electron microscopy (SEM; Hitachi, S-4800) and transmission electron microscopy (HRTEM; Talos F200S*) were used to observe the morphology of the nanomaterials. The composition of the fibers was studied by Fourier transform infrared spectroscopy (FT-IR; Nicolet 6700) and X-ray photo spectroscopy (XPS; AXIS Ultra DLD).

For TEM characterization, the PPy-coated GC plate was electrolyzed at -0.7 V for certain times (50, 100, 200, 300 s). After washing with copious 0.1 M H_2SO_4 and water successively, the PPy-Cu sample was carefully collected by scratching out of the GC surface and then dispersed in ethanol solution by sonification.

Analytical method

The electrochemical experiments were carried out using CHI 760D electrochemical workstation (Shanghai Chen Hua CHI Instrument Company) with a three-electrode system including a GCE working electrode, an Ag/AgCl (3 M KCl) reference electrode, and a Pt counter electrode.

The electrochemical behavior of the work electrodes was investigated by cyclic voltammetry (CV). All the CV signals reached a steady state in 5 cycles of scans. The current response of PPy-Cu/GCE to nitrite was recorded by i-t curve at -0.4 V.

Results and discussion

Formation and analysis of PPy nanotubes

Polymerization of Py and the formation of PPy nanotubes were characterized by FT-IR. The spectra of sulfonated PS, PS/PPy, and hollow PPy nanotubes are shown in Fig. 1. The absorption bands at 1494, 1452, 754, and 694 cm^{-1} correspond to the C=C framework of benzene, methylene, and methane groups in PS [39]. The absorption peaks at 1180, 1070, and 1035 cm^{-1} are related to the stretching vibration of sulfonic group [40, 41], indicating that the sulfonic groups have been successfully grafted to the PS fiber surface. The presence of the $-SO_3^-$ ensures that the Py monomer can be adsorbed stably and uniformly on the surface of the PS nanofibers. After polymerization of Py, two new peaks appear at 1566 and 1550 cm^{-1} , corresponding to the characteristic absorption peaks of C=C and C–C stretching vibration of PPy,

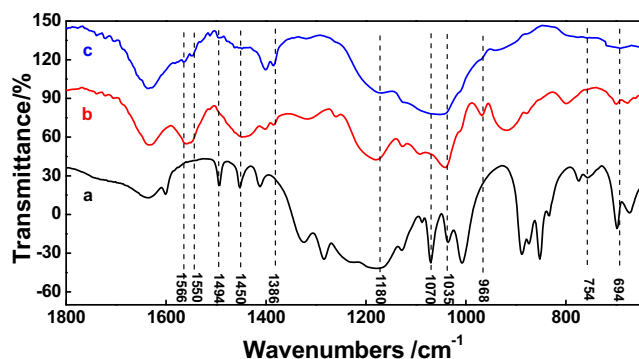


Fig. 1 FT-IR spectra of three different nanofibers. a Sulfonated PS nanofibers. b PS/PPy composites. c PPy nanotubes

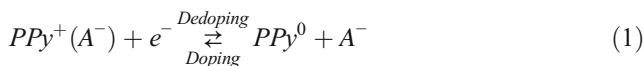
respectively [42]. New absorption bands at 1386 and 968 cm^{-1} are found, which are ascribed to the C–N stretching vibration and the in-plane deformation vibration of N–H, respectively [42]. These confirm the formation of PPy polymer on the PS surface. After THF washing, the characteristic absorption bands of PS at 754 and 694 cm^{-1} disappear, demonstrating that the PS nanofibers are removed with THF washing. However, the absorption peaks at 1180, 1070, and 1035 cm^{-1} representing the sulfonic group on the PPy nanotubes still exist, indicating that some sulfonic ions are doped into the PPy chain. It concludes the PPy nanotubes in oxidation state are formed successfully.

Figure 2A displays the morphology of PS nanofibers with an average diameter of 150 nm. After polymerization of Py, the fibers maintain the original continuous and uniform structure, but the surface becomes a bit coarser and rougher (Fig. 2B). Through THF etching, the tubular PPy is found clearly from the cross-section image of SEM (inset of Fig. 2C). This indicates the formation of PPy nanotubes.

Various PPy nanotubes were obtained by varying the concentration of Py monomer (0.2%, 0.4%, 0.6%, 0.8%) during polymerization. Figure 3 presents the cross-section images of different PPy tubes. It can be seen from Fig. 3A that the surface of the PPy(0.2) nanotubes is grainy and rough with an average wall thickness of 80 nm. With increasing the concentration of Py, the obtained PPy nanotubes become well-defined, and the surface is uniform with some pores (Fig. 3B, C). It is possible that few PPy nuclei are formed at low concentration, leading to large particles, and thus the PPy nanotube is poor-defined. However, high concentration (0.8%) of Py leads to agglomeration of PPy particles and thick wall (Fig. 3D).

Electrochemistry of PPy/GCE and Cu deposition on PPy/GCE

As demonstrated in SEM, various Py monomer concentrations lead to different morphologies of PPy nanotubes. CV is applied to investigate the redox properties of various PPy/GCEs. Figure 4A presents the CV curves of the PPy/GCEs coated with same mass but different PPy structure. Compared with bare GCE (curve a), there is a broad redox peak at round 0 V, which corresponds to the redox doping and dedoping of PPy. The reaction is described as below [43]:



The PPy/GCE obtained with well-defined PPy nanotubes presents higher redox current, indicating the large specific surface and better electron transfer of the PPy nanotube (vide supra).

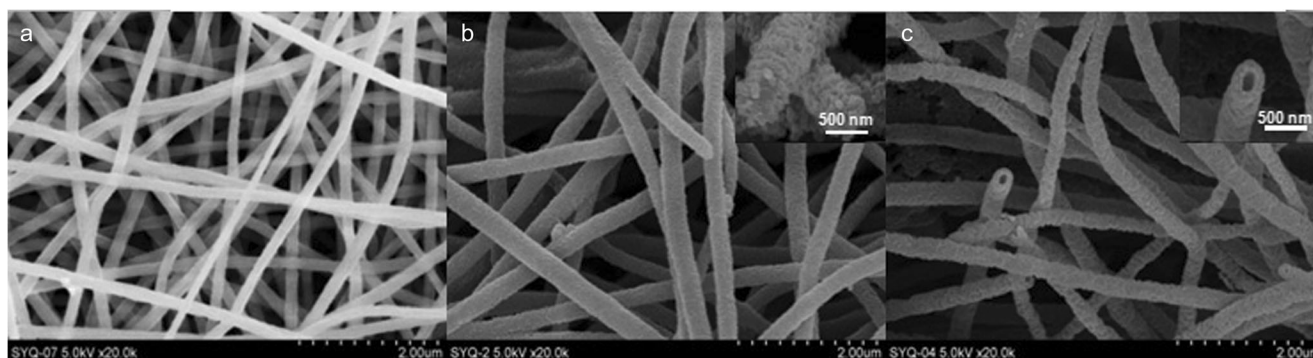
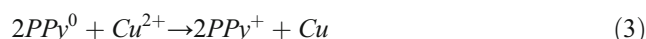


Fig. 2 SEM images of three different nanofibers. **a** PS nanofibers. **b** PS/PPy composites. **c** PPy nanotubes. Inset is the cross-section image (upper right)

The PPy-modified GCE with large specific surface area is supposed to facilitate the deposition of Cu due to Cu-PPy interaction and reducing property of PPy [33, 44, 45]. The deposition of Cu on PPy/GCEs is performed in 0.1 M H_2SO_4 solution containing 0.05 M $CuSO_4$ and 1 mM KCl. Figure 4B exhibits the CV curves of Cu/GCE and various PPy-Cu/GCEs. In the absence of PPy, very weak reduction and oxidation signals of Cu are found at about -0.16 and 0 V. It indicates that very low amount of Cu is deposited on bare GCE (curve a). In contrast, the redox signal of Cu is enhanced dramatically in the presence of PPy, and the highest peak is observed on PPy(0.6)-Cu/GCE, with the peak-peak separation of 200 mV. Under the polarization condition for Cu deposition, the oxidized PPy is reduced, and the reduced state PPy^0 promotes the reduction of Cu [44]. The reaction can be described in the following equation.



The PPy nanotube with large specific surface area facilitates the charge transfer. Therefore, the deposition of Cu on PPy nanotube electrode is highly promoted. The peak current and reversibility of signal are highly dependent on the morphology of PPy. The current intensity of Cu arrives at the maximum at the PPy(0.6)/GCE with the same coating mass of PPy tube, because the PPy(0.6) nanotube is much uniform and well-defined, compared to other PPy nanotubes (see SEM in Fig. 3). It concludes that the well-defined PPy tube with uniform surface possesses higher active sites, facilitating the adsorption and deposition of Cu, being consistent with the CV in Fig. 4A.

Fig. 3 Cross-section SEM images of PPy nanotubes prepared with different concentrations of pyrrole: 0.2% (a), 0.4% (b), 0.6% (c), and 0.8% (d)

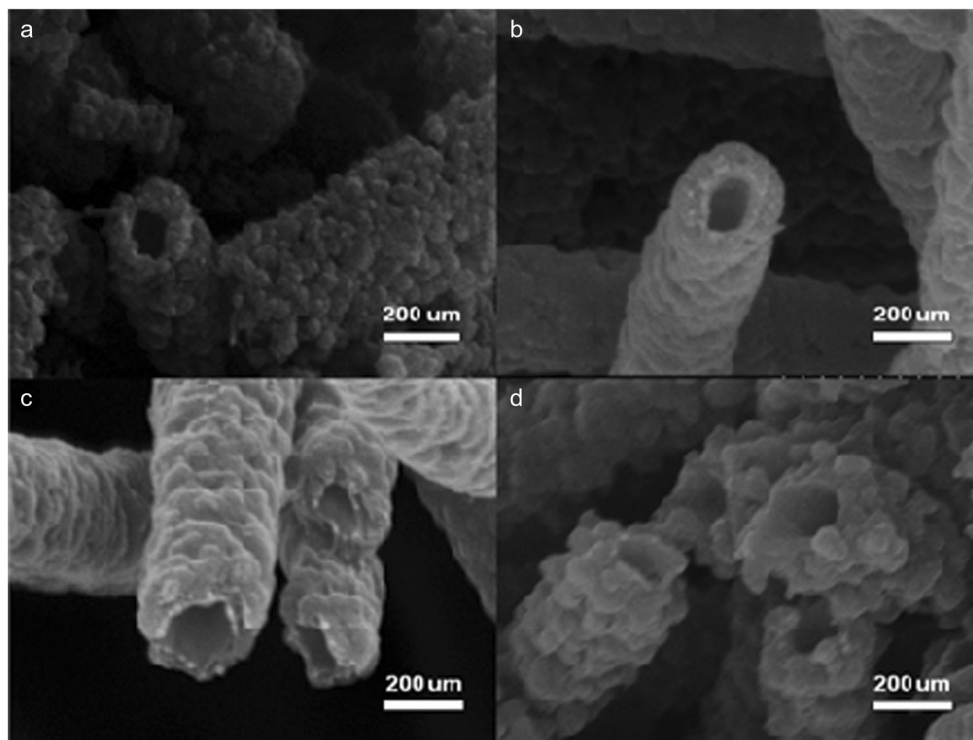


Fig. 4 CVs of bare GCE (a) and PPy/GCEs (b–e). **b** CVs of Cu/GCE (a) and PPy-Cu/GCEs (b–e). Curve (b–e): PPy(0.2), PPy(0.4), PPy(0.6), and PPy(0.8). Electrolyte: 0.1 M H₂SO₄, scan rate: 50 mV/s

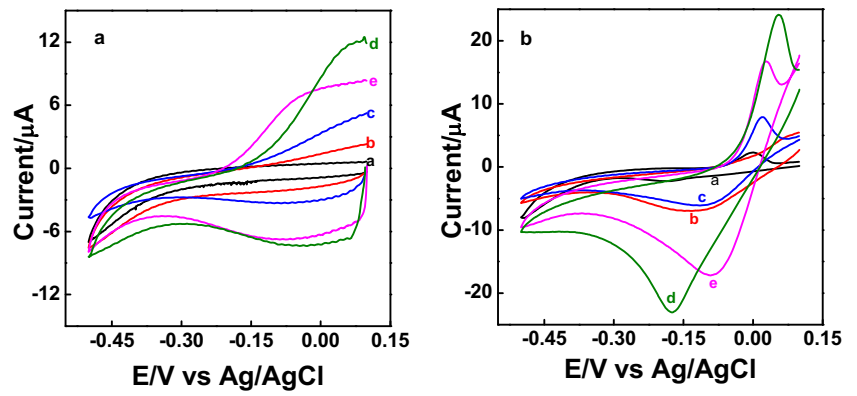
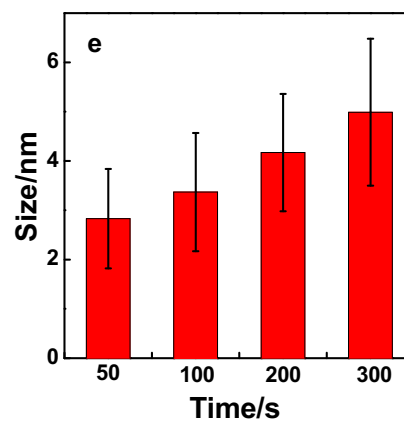
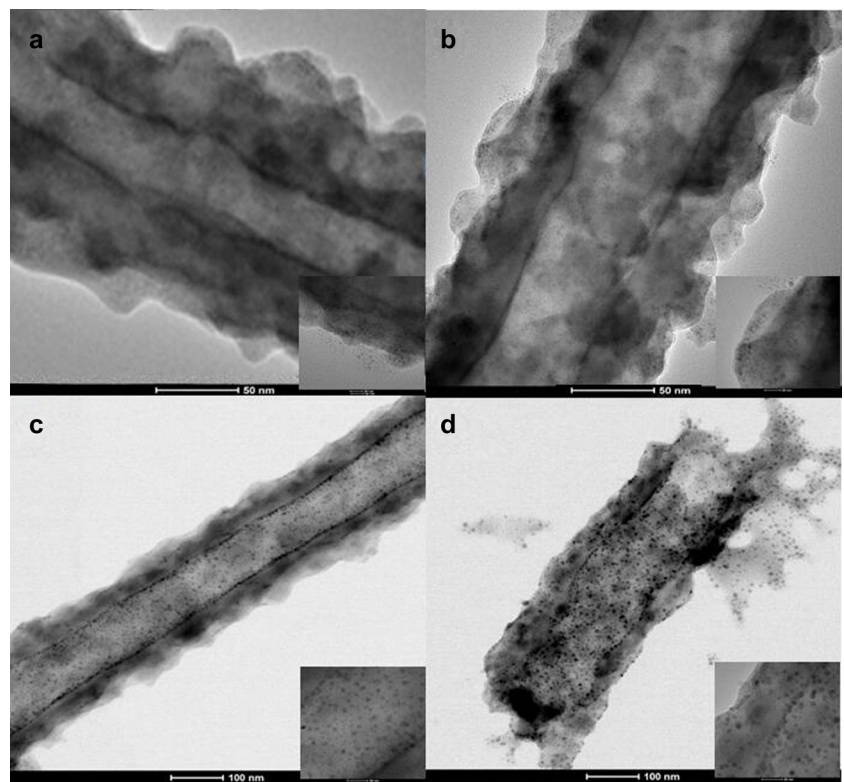


Fig. 5 TEM images of PPy-Cu at different deposition times of Cu of 50 s (a), 100 s (b), 200 s (c), and 300 s (d). Scale bar: 50 nm for a and b; 100 nm for c and d; 20 nm in the insets of a–d. e The average copper size at different deposition times



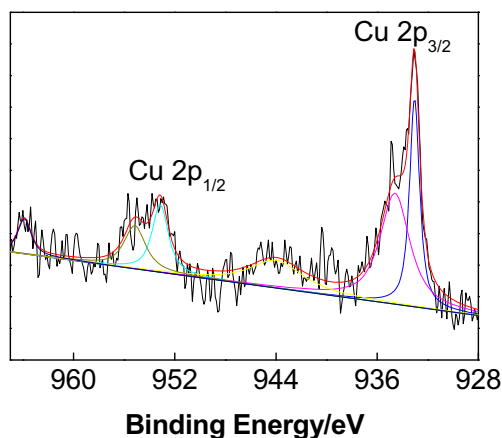


Fig. 6 Cu2p high-resolution XPS scan of PPy-Cu

Effect of Cu deposition time

By changing the Cu deposition time, Cu nanoparticles with different sizes were obtained. Figure 5A–D shows the TEM images of PPy-Cu with various deposition times. Ultrafine Cu particles are uniformly decorated on the PPy surface. As the deposition time increases, there are more and more Cu particles observed and the particle size is slightly increasing (insets of patterns A–D). When the deposition time increases to 300 s, there is a little agglomeration between Cu particles (Fig. 5D). The relationship of particle size with deposition time is drawn in Fig. 5E. The average particle size is 4.2 ± 1.2 nm at the electrolysis time of 200 s. The uniform distribution of Cu and increase of Cu content with increasing

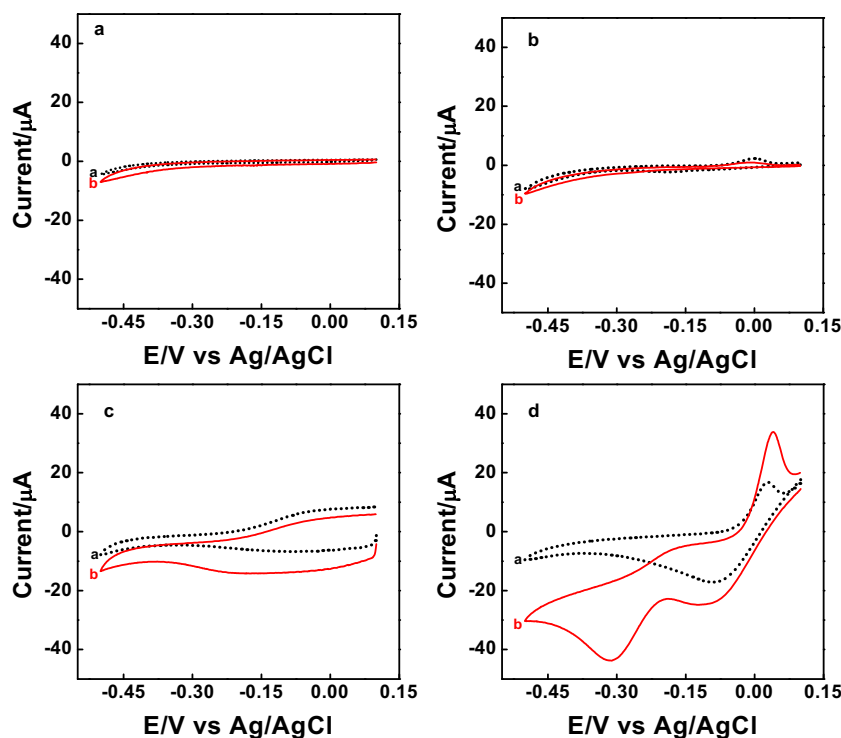
deposition time have been demonstrated by TEM mapping and energy-dispersive X-ray analysis (details in Fig. S2 and Table S1 in supporting information).

In order to analyze the valence state of copper, XPS characterization of PPy-Cu sample was performed. Figure 6 shows the high-resolution scan spectrum of Cu2p. By least square fitting, Cu2p_{3/2} and Cu2p_{1/2} at 933.0 and 953.1 eV, corresponding to zero-valence Cu [46], are observed. In addition, four weak peaks are found at 934.6, 944.0, 955.1, and 963.7 eV, which are the characteristic peaks of Cu2p in CuO [47, 48], indicating the presence of a little CuO due to partial oxidation of Cu. The result shows that zero-valence Cu is dominated in PPy-Cu.

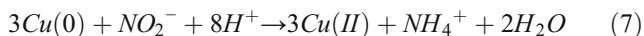
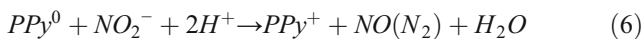
Electrocatalytic reduction of nitrite

Electrode materials play a significant role on the reduction of nitrite. Figure 7 shows the CV curves of various electrodes in 0.1 M H₂SO₄ solution in the absence and presence of 0.5 mM NO₂⁻. There is negligible response on GCE (a). And the catalytic response of Cu/GCE to the reduction of nitrite is not found due to very small deposition amount of Cu (b). On PPy/GCE (c), the reduction current increases slightly upon the addition of nitrite, while the PPy-Cu/GCE (d) shows a dramatic enhancement of the catalytic current at -0.3 V. It is known that PPy can catalyze the reduction of nitrite during the dedoping process of PPy [49]. Meanwhile, the Cu nanoparticles on PPy-Cu/GCE can also function as a catalyst for nitrite reduction

Fig. 7 CVs of GCE (a), Cu/GCE (b), PPy/GCE (c), and PPy-Cu/GCE (d) in the absence (a) and presence (b) of 0.5 mM nitrite in 0.1 M H₂SO₄ recorded at 50 mV/s



[50]. The nitrite reduction mechanism on the PPy-Cu/GCE can be described with the following equations:



The thus-synthesized PPy is in its oxidation state (PPy⁺) which can accumulate and adsorb NO₂⁻ on the active sites of PPy⁺. Upon applying a negative potential, PPy⁺ is reduced into PPy⁰, which further catalyzed the reduction of nitrite into NO or N₂ (Eq. 6). On the other hand, Cu (0) in the PPy-Cu composite not only has good conductivity to promote the electron transfer of PPy, but also functions as a reducing agent catalyzing the reduction of nitrite, as shown in Eq. 7 [51]. Therefore, the synergetic effect in the PPy-Cu composite contributes much to its high catalytic activity towards the reduction of nitrite.

As discussed previously, PPy formed by different concentrations of Py exhibits various morphologies, and the resultant PPy electrodes possess different electrochemical activities (Fig. 4). The catalytic sensitivity of the various PPy-Cu/GCEs to nitrite reduction is investigated by measuring the calibration curves through CV scan in different concentrations of nitrite. Figure 8 shows the sensitivity at different electrodes. Being consistent with the redox response of PPy on electrodes, the corresponding sensitivity to nitrite reduction increases with the Py monomer and arrives at the maximum on the PPy(0.6)-Cu/GCE. It indicates that the increase in the copper deposition amount on the well-defined PPy tubes led to the enhancement of catalytic sensitivity. However, poorly defined PPy morphology (Py 0.8%) is not favorable to Cu deposition, and thus, the low Cu deposition and low

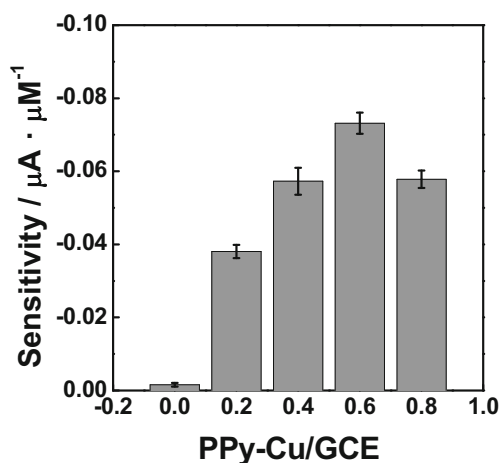


Fig. 8 The sensitivity for nitrite ions on various PPy-Cu/GCEs (PPy(0.2), PPy(0.4), PPy (0.6), and PPy (0.8))

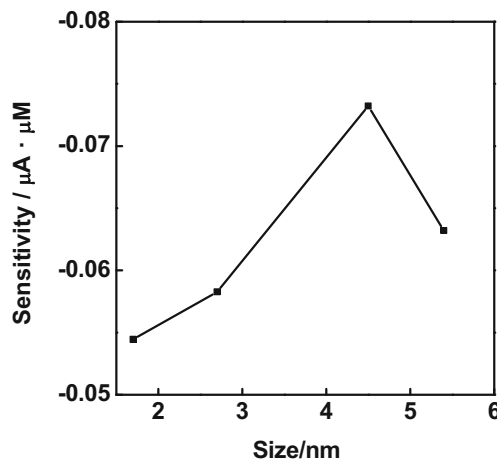


Fig. 9 The sensitivity of PPy-Cu/GCE to nitrite ions with different sizes of Cu

sensitivity to nitrite reduction are observed at PPy(0.8)-Cu/GCE. The PPy(0.6)-Cu/GCE has the best sensitivity compared to other electrodes. In the subsequent experiments, the PPy(0.6)-Cu/GCE is used for nitrite measurement.

Effect of copper size and solution pH on nitrite reduction at the PPy-Cu/GCE

As discussed in TEM analysis, the fine Cu particles with different sizes can be obtained by adjusting the deposition times. Nitrite reduction on PPy-Cu/GCE with different sizes was investigated and the results are shown in Fig. 9. The catalytic reduction current of nitrite increases with the deposition time of Cu particles and arrives at the highest when PPy-Cu is obtained with the deposition time of 200 s. Longer deposition time leads to the decreased catalytic current, which is probably due to larger Cu particle size and the agglomeration of Cu (shown in Table S1). It concludes that the catalytic reduction

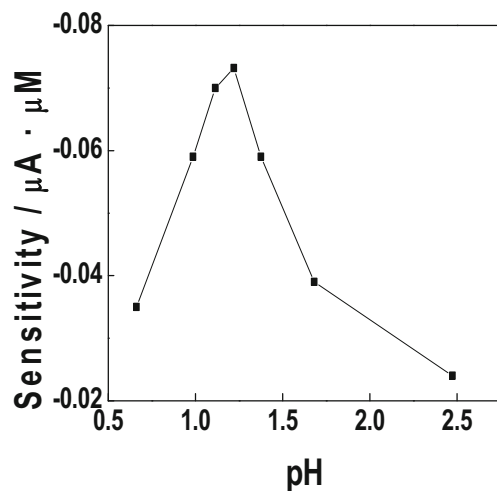
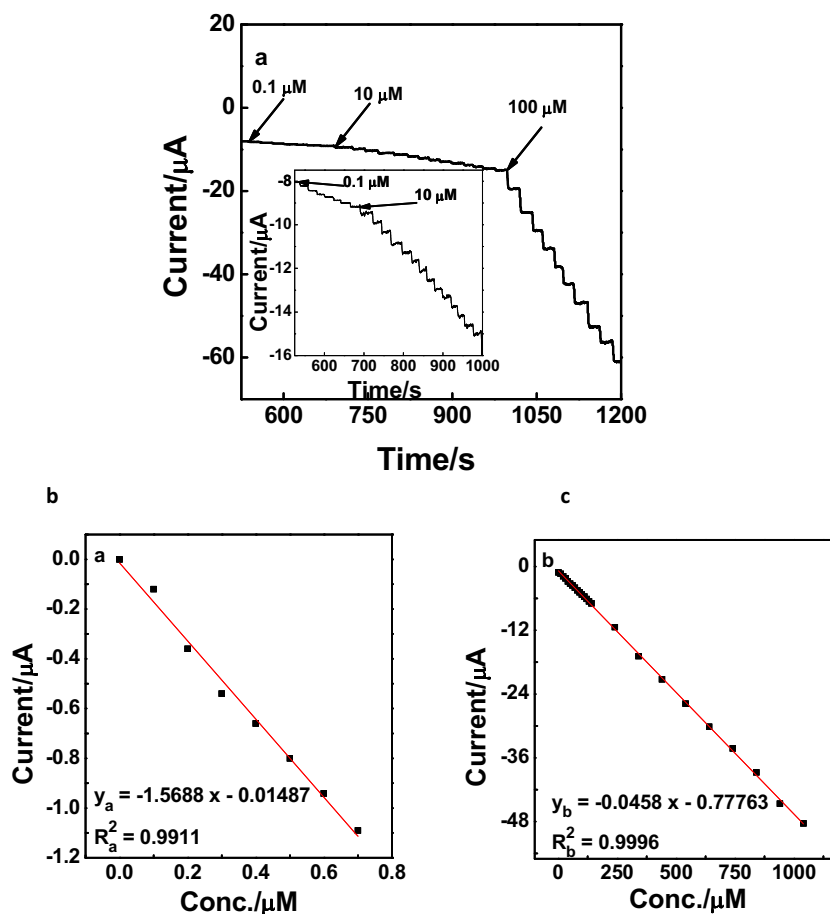


Fig. 10 The sensitivity of PPy-Cu/GCE to nitrite ions in electrolyte with different pH values

Fig. 11 a Amperometric responses of PPy-Cu/GCE on successive injection of nitrite into 0.1 M H₂SO₄. Applied potential: -0.4 V. The corresponding calibration plots of current response versus nitrite concentration at different concentrations in the range of 0 to 0.7 μM (**b**) and 0.7 to 1040.7 μM (**c**)



of nitrite by PPy-Cu/GCE is closely related to the Cu amount and Cu particle size, which is consistent with the morphological changes in the TEM image of Fig. 5A–D.

The catalytic reduction performance of the PPy-Cu/GCE was studied in different concentrations of H₂SO₄ solution (different pH) and the corresponding catalytic sensitivities were obtained

by CV. As shown in Fig. 10, the catalytic sensitivity of the PPy-Cu/GCE to nitrite reduction increases with pH decreasing at high pH range (from pH 2.5 to pH 1.22), while decreases when pH is lower than 1.22. It is reasonable that the presence of H⁺ facilitates the catalytic reduction of nitrite on PPy-Cu, as stated in Eqs. 6 and 7. However, excessive acidity leads to severe

Table 1 Comparison of catalytic performance of various nitrite sensors

Electrode	Limit of detection (μM)	Linear range (μM)	References
Cu-MWCNT-RGO/GCE	0.03	0.1–75	[18]
GR-PPy-CS/GCE	0.1	0.5–722	[49]
Cu/GCE	20	50–30,000	[50]
Cu-NDs/RGO/GCE	1.25	1.25–13,000	[51]
CuNp-CNTs/GCE	0.08	1–600	[52]
CuNp-Au/GCE	0.1	0.1–300	[53]
Cu ^{II} -DHB/CPE	0.05	0.2–2	[54]
Cu-MPS/CPE	0.09	0.25–120	[55]
NaR-SOD-CNT-PPy/Pt	0.05	0.1–1000	[56]
PPy-Cu _{nano} /GCE	0.03	0.1–0.7 0.7–1040.7	This work

MWCNT multi-walled carbon nanotubes, NDs nanodendrites, RGO reduced graphene oxide, CNT carbon nanotube, Np nanoparticle, GR graphene, CS chitosan, DHB N,N'-bis (2,5-dihydroxybenzylidene)-1,2-diaminoethane, MPS (3-mercaptopropyl) trimethoxysilane, NaR nitrate reductase, SOD superoxide dismutase

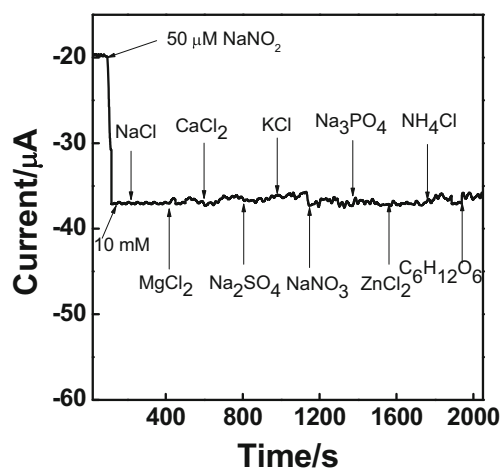


Fig. 12 Amperometric responses of PPy-Cu/GCE on successive injection of 200-fold of NaCl, MgCl₂, CaCl₂, Na₂SO₄, KCl, NaNO₃, Na₃PO₄, ZnCl₂, NH₄Cl, and C₆H₁₂O₆ into 0.1 M H₂SO₄. Applied potential: -0.4 V

hydrogen evolution reaction, thereby reducing the catalytic performance of nitrite. In the following experiments, pH 1.22 solution was used for further measurement.

Amperometric determination of nitrite at the PPy-Cu/GCE

In order to further analyze the catalytic property of the PPy-Cu/GCE, the amperometric response is obtained in 0.1 M H₂SO₄ at a constant potential of -0.4 V. Figure 11A shows the typical *i-t* curve with successive increments of nitrite under stirring condition. The reduction current increases steeply upon addition of nitrite and arrives at a platform in less than 3 s, indicating a rapid diffusion of nitrite to the PPy-Cu/GCE. A steady increase of current is observed in a wide concentration range from 0.1 to 0.7 μM. The corresponding calibration plots are shown in Fig. 11B, C with concentration ranging in 0.1~0.7 and 0.7~1040.7 μM, respectively. The corresponding calibration equations are calculated to be $ip_a (\mu A) = -1.5688 C - 0.01487$ ($R_a^2 = 0.9911$) and $ip_c (\mu A) = -0.0458 C - 0.77763$ ($R_c^2 = 0.9996$). The limit of detection is about 0.03 μM ($S/N > 3$). The analysis performances of this proposed material for nitrite determination together with other materials previously reported are listed in Table 1 for comparison. It demonstrates that the current PPy-Cu/GCE possesses the wide linear range and low detection limit compared with the state of the art [52–56].

Table 2 NO₂⁻ determination (μM) and spiked recovery test in real samples ($N = 3$) on the PPy-Cu/GCE under the optimal conditions

Sample	Added	Found (μM)	Recovery (%)	RSD (%)	UV-Vis (μM)
Well water	0	0.18 ± 0.08	/	2.3	0.11 ± 0.06
	0.1	0.27 ± 0.10	90	2.6	0.22 ± 0.09
Lake water	0	1.35 ± 0.13	/	2.8	1.27 ± 0.15
	1.0	2.32 ± 0.21	97	3.3	2.15 ± 0.32

Anti-interference ability, stability, and reproducibility of PPy-Cu/GCE

The common interfering substances were investigated. Figure 12 is the amperometric response of PPy-Cu/GCE by adding various interfering substances (NaCl, MgCl₂, CaCl₂, Na₂SO₄, KCl, NaNO₃, Na₃PO₄, ZnCl₂, NH₄Cl, and C₆H₁₂O₆) successively to 0.1 M H₂SO₄ containing 0.05 mM nitrite. It can be seen that there is no obvious current response after adding 200-fold of the above substances (shown in Table S2). It concludes that PPy-Cu/GCE has good selectivity for nitrite measurement.

The long-term stability and reproducibility of PPy-Cu/GCE were further evaluated. After leaving the electrode in air for 1 month, the current response can maintain 90% for 0.5 mM nitrite, manifesting that PPy-Cu/GCE has good stability. In addition, the relative standard deviation (RSD) for six individual PPy-Cu/GCEs is 8.8% by assaying 0.5 mM nitrite with the same method. For six consecutive parallel determinations in 0.5 mM nitrite using the same modified electrode, the RSD of the corresponding current response was 3.6%, indicating that the modified electrode has good reproducibility.

Real sample analysis

To evaluate the feasibility of the PPy-Cu/GCE for practical application, this electrode was applied to detect NO₂⁻ in lake water and well water samples. All the water samples were filtered through a 0.2-μm membrane and adjusted to pH 1.22 before detection. The results are shown in Table 2 ($n = 3$), which are in good agreement with the standard UV-Vis method (GB/T 5750.5-2006). The spiked water recovery experiment gives the recovery values of 90–97%. Therefore, the PPy-Cu-modified electrode has acceptable detection accuracy for NO₂⁻ in real water samples.

Conclusion

Ultrafine Cu-coated PPy nanotube has been fabricated with electrospun PS nanofibers as template followed by PPy polymerization and Cu electrochemical deposition. Py concentration has significant influence on the morphology and electrochemical properties of PPy nanotubes, thus influencing the deposition amount of Cu. The well-defined PPy tube promotes the deposition of Cu and ultrafine Cu nanoparticles

can be fine-tuned by changing deposition time of Cu. The PPy(0.6)-Cu/GCEs with 4.2 ± 1.2 nm Cu particle size (200 s deposition time) present a highly sensitive electrocatalytic performance to the reduction of nitrite, with broad linear detection ranges and low detection limit. It has been applied successfully for the real water sample analysis. The high selectivity, stability, and repeatability of the PPy-Cu/GCEs demonstrate a great potential for nitrite sensing application.

Funding information This research was supported by the National Natural Science Foundation of China (Nos. 21476047, 21776045).

References

- Du Y, Shen SZ, Cai KF, Casey PS (2012) Research progress on polymer-inorganic thermoelectric nanocomposite materials. *Prog Polym Sci* 37(6):820–841. <https://doi.org/10.1016/j.progpolymsci.2011.11.003>
- Shimomura K, Ikai T, Kanoh S, Yashima E, Maeda K (2014) Switchable enantioseparation based on macromolecular memory of a helical polyacetylene in the solid state. *Nat Chem* 6(5):429–434. <https://doi.org/10.1038/nchem.1916>
- Zeng Q, Cai P, Li Z, Qin JG, Tang BZ (2008) An imidazole-functionalized polyacetylene: convenient synthesis and selective chemosensor for metal ions and cyanide. *Chem Commun* (9): 1094–1096. <https://doi.org/10.1039/b717764j>
- Hashemi P, Bagheri H, Afkhami A, Ardakani YH, Madrakian T (2017) Fabrication of a novel aptasensor based on three-dimensional reduced graphene oxide/polyaniline/gold nanoparticle composite as a novel platform for high sensitive and specific cocaine detection. *Anal Chim Acta* 996:10–19. <https://doi.org/10.1016/j.aca.2017.10.035>
- Zhang LL, Huang D, Hu NT, Yang C, Li M, Wei H, Yang Z, Su YJ, Zhang YF (2017) Three-dimensional structures of graphene/polyaniline hybrid films constructed by steamed water for high-performance supercapacitors. *J Power Sources* 342:1–8. doi: 10.1016/j.jpowsour.2016. 11.068
- Baker CO, Huang X, Nelson W, Kaner RB (2017) Polyaniline nanofibers: broadening applications for conducting polymers. *Chem Soc Rev* 46(5):1510–1525. <https://doi.org/10.1039/c6cs00555a>
- Amidi S, Ardakani YH, Amiri-Aref M, Ranjbari E, Sepehri Z, Bagheri H (2017) Sensitive electrochemical determination of rifampicin using gold nanoparticles/poly-melamine nanocomposite. *RSC Adv* 7(64):40111–40118. <https://doi.org/10.1039/c7ra04865c>
- Sepehri Z, Bagheri H, Ranjbari E, Amiri-Aref M, Amidi S, Rouini MR, Ardakani YH (2017) Simultaneous electrochemical determination of isoniazid and ethambutol using poly-melamine/electrodeposited gold nanoparticles modified pre-anodized glassy carbon electrode. *Ionics*. <https://doi.org/10.1007/s11581-017-2263-y>
- Molaei K, Bagheri H, Asgharinezhad AA, Ebrahimzadeh H, Shamsipur M (2017) SiO₂-coated magnetic graphene oxide modified with polypyrrole-polythiophene: a novel and efficient nanocomposite for solid phase extraction of trace amounts of heavy metals. *Talanta* 167:607–616. <https://doi.org/10.1016/j.talanta.2017.02.066>
- Jeon SS, Kim C, Ko J, Im SS (2011) Pt nanoparticles supported on polypyrrole nanospheres as a catalytic counter electrode for dye-sensitized solar cells. *J Phys Chem C* 115(44):22035–22039. <https://doi.org/10.1021/jp206535c>
- Ohkita H, Cook S, Astuti Y, Duffy W, Tierney S, Zhang W, Heeney M, McCulloch I, Nelson J, Bradley DDC, Durrant JR (2008) Charge carrier formation in polythiophene/fullerene blend films studied by transient absorption spectroscopy. *J Am Chem Soc* 130(10):3030–3042. <https://doi.org/10.1021/ja076568q>
- Ghoorchian M, Tavoli F, Alizadeh N (2017) Long-term stability of nanostructured polypyrrole electrochromic devices by using deep eutectic solvents. *J Electroanal Chem* 807:70–75. <https://doi.org/10.1016/j.jelechem.2017.11.026>
- Shih HK, Chen YH, Chu YL, Cheng CC, Chang FC, Zhu CY, Kuo SW (2015) Photo-crosslinking of pendent uracil units provides supramolecular hole injection/transport conducting polymers for highly efficient light-emitting diodes. *Polymers* 7(5):804–818. <https://doi.org/10.3390/polym7050804>
- Sumanta S, Saptarshi D, Goutam H, Pallab B, Chapal KD (2013) Graphene/polypyrrole nanofiber nanocomposite as electrode material for electrochemical supercapacitor. *Polymer* 54(3):1033–1042. <https://doi.org/10.1016/j.polymer.2012.12.042>
- Bose S, Kim NH, Kuila T, Lau KT, Lee JH (2011) Electrochemical performance of a graphene-polypyrrole nanocomposite as a supercapacitor electrode. *Nanotechnology* 22(29):9. <https://doi.org/10.1088/0957-4484/22/29/295202>
- Park H, Kim Y, Choi YS, Hong WH, Jung D (2008) Surface chemistry and physical properties of Nafion/polypyrrole/Pt composite membrane prepared by chemical in situ polymerization for DMFC. *J Power Sources* 178(2):610–619. <https://doi.org/10.1016/j.jpowsour.2007.08.050>
- Morozaan A, Jegou P, Campidelli S, Palacin S, Jousset B (2012) Relationship between polypyrrole morphology and electrochemical activity towards oxygen reduction reaction. *Chem Commun* 48(38):4627–4629. <https://doi.org/10.1039/c2cc30871a>
- Bagheri H, Hajian A, Rezaei M, Shirzadmehr A (2017) Composite of Cu metal nanoparticles-multiwall carbon nanotubes-reduced graphene oxide as a novel and high performance platform of the electrochemical sensor for simultaneous determination of nitrite and nitrate. *J Hazard Mater* 324:762–772. <https://doi.org/10.1016/j.jhazmat.2016.11.055>
- Fu YZ, Manthiram A (2012) Core-shell structured sulfur-polypyrrole composite cathodes for lithium-sulfur batteries. *RSC Adv* 2(14):5927–5929. <https://doi.org/10.1039/c2ra20393f>
- Li J, Lin XQ (2007) Glucose biosensor based on immobilization of glucose oxidase in poly(o-aminophenol) film on polypyrrole-Pt nanocomposite modified glassy carbon electrode. *Biosens Bioelectron* 22(12):2898–2905. <https://doi.org/10.1016/j.bios.2006.12.004>
- Liu FJ, Yuan Y, Li L, Shang SM, Yu XH, Zhang Q, Jiang SX, Wu YG (2015) Synthesis of polypyrrole nanocomposites decorated with silver nanoparticles with electrocatalysis and antibacterial property. *Compos Pt B-Eng* 69:232–236. <https://doi.org/10.1016/j.compositesb.2014.09.030>
- Dubal DP, Chodankar NR, Caban HZ, Wolfart F, Vidotti M, Holze R, Lokhande CD, Gomez RP (2016) Synthetic approach from polypyrrole nanotubes to nitrogen doped pyrolyzed carbon nanotubes for asymmetric supercapacitors. *J Power Sources* 308:158–165. <https://doi.org/10.1016/j.jpowsour.2016.01.074>
- Liu JY, Qiu JX, Miao YQ, Chen JR (2008) Preparation and characterization of Pt-polypyrrole nanocomposite for electrochemical reduction of oxygen. *J Mater Sci* 43(18):6285–6288. <https://doi.org/10.1007/s10853-008-2905-6>
- Tsakova V (2008) How to affect number, size, and location of metal particles deposited in conducting polymer layers. *J Solid State Electrochem* 12(11):1421–1434. <https://doi.org/10.1007/s10008-007-0494-y>
- Ulubay S, Dursun Z (2010) Cu nanoparticles incorporated polypyrrole modified GCE for sensitive simultaneous determination of dopamine and uric acid. *Talanta* 80(3):1461–1466. <https://doi.org/10.1016/j.talanta.2009.09.054>
- Singh A, Salmi Z, Joshi N, Jha P, Decorse P, Lecoq H, Lau-Truong S, Jouini M, Aswal DK, Chehimi MM (2013) Electrochemical investigation of free-standing polypyrrole-silver nanocomposite

- films: a substrate free electrode material for supercapacitors. *RSC Adv* 3(46):24567–24575. <https://doi.org/10.1039/c3ra42786b>
27. Hnida KE, Socha RP, Sulka GD (2013) Polypyrrole-silver composite nanowire arrays by cathodic Co-deposition and their electrochemical properties. *J Phys Chem C* 117(38):19382–19392. <https://doi.org/10.1021/jp4038304>
 28. Lakshinandan G, Neelotpal SS, Chowdhury D (2011) Determining the ionic and electronic contribution in conductivity of polypyrrole/Au nanocomposites. *J Phys Chem C* 115(40):19668–19675. <https://doi.org/10.1021/jp2075012>
 29. Chen W, Li CM, Yu L, Lu ZS, Zhou Q (2008) In situ AFM study of electrochemical synthesis of polypyrrole/Au nanocomposite. *Electrochem Commun* 10(9):1340–1343. <https://doi.org/10.1016/j.elecom.2008.07.001>
 30. Subramanyam K, Niteen J, Victoria JG (2016) In situ preparation and characterization of a conductive and magnetic nanocomposite of polypyrrole and copper hydroxychloride. *RSC Adv* 6(2):967–977. <https://doi.org/10.1039/c5ra20441k>
 31. Nia PM, Meng WP, Lorestani F, Mahmoudian MR, Alias Y (2015) Electrodeposition of copper oxide/polypyrrole/reduced graphene oxide as a nonenzymatic glucose biosensor. *Sens Actuatur B-Chem* 209:100–108. <https://doi.org/10.1016/j.snb.2014.11.072>
 32. Bagheri H, Afkhami A, Khoshafar H, Hajian A, Shahriyari A (2017) Protein capped Cu nanoclusters-SWCNT nanocomposite as a novel candidate of high performance platform for organophosphates enzymeless biosensor. *Biosensors & bioelectronics* 89 (Pt 2):829–836. doi:<https://doi.org/10.1016/j.bios.2016.10.003>
 33. Makhloufi L, Hammache H, Saidani B, Akilal N, Maloum Y (2000) Preparation on iron of a polypyrrole (PPy) electrode modified with copper by the electrochemical cementation process. *J Appl Electrochem* 30(10):1143–1150. <https://doi.org/10.1023/a:1004098805227>
 34. Lu YC, Zheng QQ, Wu J, Yu YH (2018) Enhanced electrochemical charge storage performance by doping of copper phthalocyanine-3, 4',4'',4'''-tetrasulfonic acid tetrasodium salt into polypyrrole/multi-walled carbon nanotubes 3D-nanostructured electrodes. *Electrochim Acta* 265:594–600. <https://doi.org/10.1016/j.electacta.2018.01.173>
 35. Majumder M, Choudhary RB, Thakur AK, Karbhal I (2017) Impact of rare-earth metal oxide (Eu_2O_3) on the electrochemical properties of a polypyrrole/CuO polymeric composite for supercapacitor applications. *RSC Adv* 7(32):20037–20048. <https://doi.org/10.1039/c7ra01438d>
 36. Liu J, Zhu G, Li X, Batchelor McAuley C, Sokolov SV, Compton RG (2017) Quantifying charge transfer to nanostructures: polyaniline nanotubes. *Applied Materials Today* 7:239–245. <https://doi.org/10.1016/j.apmt.2017.04.008>
 37. Bagheri H, Khoshafar H, Afkhami A, Amidi S (2016) Sensitive and simple simultaneous determination of morphine and codeine using a Zn_2SnO_4 nanoparticle/graphene composite modified electrochemical sensor. *New J Chem* 40(8):7102–7112. <https://doi.org/10.1039/c6nj00505e>
 38. Lee HK, Yang DS, Oh W, Choi SJ (2016) Copper ferrocyanide functionalized core-shell magnetic silica composites for the selective removal of cesium ions from radioactive liquid waste. *J Nanosci Nanotechnol* 16(6):6223–6230. <https://doi.org/10.1166/jnn.2016.10886>
 39. Sertchook H, Avnir D (2003) Submicron silica/polystyrene composite particles prepared by a one-step sol-gel process. *Chem Mater* 15(8):1690–1694. <https://doi.org/10.1021/cm020980h>
 40. Lu GW, Li C, Shi GQ (2006) Polypyrrole micro- and nanowires synthesized by electrochemical polymerization of pyrrole in the aqueous solutions of pyrenesulfonic acid. *Polymer* 47(6):1778–1784. <https://doi.org/10.1016/j.polymer.2006.01.081>
 41. Yang Y, Chu Y, Yang FY, Zhang YP (2005) Uniform hollow conductive polymer microspheres synthesized with the sulfonated polystyrene template. *Mater Chem Phys* 92(1):164–171. <https://doi.org/10.1016/j.matchemphys.2005.01.007>
 42. Li X, Wan MX, Wei Y, Shen JY, Chen ZJ (2006) Electromagnetic functionalized and core-shell micro/nanostructured polypyrrole composites. *J Phys Chem B* 110(30):14623–14626. <https://doi.org/10.1021/jp062339z>
 43. Liu J, Wan MX (2001) Polypyrrole doped with 1,5-naphthalenedisulfonic acid. *Synth Met* 124(2–3):317–321. [https://doi.org/10.1016/s0379-6779\(01\)00372-1](https://doi.org/10.1016/s0379-6779(01)00372-1)
 44. Zhang TT, Yuan R, Chai YQ, Li WJ, Ling SJ (2008) A novel nonenzymatic hydrogen peroxide sensor based on a polypyrrole nanowire-copper nanocomposite modified gold electrode. *Sensors* 8(8):5141–5152. <https://doi.org/10.3390/s8085141>
 45. Liu YC, Yang KH, Ger MD (2002) Mechanism of underpotential deposition of metal on conducting polymers. *Synth Met* 126(2–3):337–345. [https://doi.org/10.1016/s0379-6779\(01\)00581-1](https://doi.org/10.1016/s0379-6779(01)00581-1)
 46. Ghodselahi T, Vesaghi MA, Shafiekhani A, Baghizadeh A, Lameii M (2008) XPS study of the $\text{Cu}@\text{Cu}_2\text{O}$ core-shell nanoparticles. *Appl Surf Sci* 255(5):2730–2734. <https://doi.org/10.1016/j.apsusc.2008.08.110>
 47. Sekar R (2017) Synergistic effect of additives on electrodeposition of copper from cyanide-free electrolytes and its structural and morphological characteristics. *Trans Nonferrous Metals Soc China* 27(7):1665–1676. [https://doi.org/10.1016/s1003-6326\(17\)60189-4](https://doi.org/10.1016/s1003-6326(17)60189-4)
 48. Ghijsen J, Tjeng LH, Van EJ, Eskes H, Westerink J, Sawatzky GA, Czyzyk MT (1988) Electronic structure of Cu_2O and CuO . *Phys Rev B* 38(16):11322–11330. <https://doi.org/10.1103/PhysRevB.38.11322>
 49. Ye DX, Luo LQ, Ding YP, Chen Q, Liu X (2011) A novel nitrite sensor based on graphene/polypyrrole/chitosan nanocomposite modified glassy carbon electrode. *Analyst* 136(21):4563–4569. <https://doi.org/10.1039/c1an15486a>
 50. Wang HY, Huang YG, Tan Z, Hu XY (2004) Fabrication and characterization of copper nanoparticle thin-films and the electrocatalytic behavior. *Anal Chim Acta* 526(1):13–17. <https://doi.org/10.1016/j.aca.2004.08.060>
 51. Zhang D, Fang YX, Miao ZY, Ma M, Du X, Takahashi S, Anzai J, Chen Q (2013) Direct electrodeposition of reduced graphene oxide and dendritic copper nanoclusters on glassy carbon electrode for electrochemical detection of nitrite. *Electrochim Acta* 107:656–663. <https://doi.org/10.1016/j.electacta.2013.06.015>
 52. Yang SL, Zeng XD, Liu XY, Wei WZ, Luo SL, Liu Y, Liu Y (2010) Electrocatalytic reduction and sensitive determination of nitrite at nano-copper coated multi-walled carbon nanotubes modified glassy carbon electrode. *J Electroanal Chem* 639(1–2):181–186. <https://doi.org/10.1016/j.jelechem.2009.11.014>
 53. Ko WY, Chen WH, Cheng CY, Lin KJ (2009) Highly electrocatalytic reduction of nitrite ions on a copper nanoparticles thin film. *Sens Actuatur B-Chem* 137(2):437–441. <https://doi.org/10.1016/j.snb.2009.01.014>
 54. Ourari A, Ketfi B, Malha SIR, Amine A (2017) Electrocatalytic reduction of nitrite and bromate and their highly sensitive determination on carbon paste electrode modified with new copper Schiff base complex. *J Electroanal Chem* 797:31–36. <https://doi.org/10.1016/j.jelechem.2017.04.046>
 55. Shiddiky MJA, Won MS, Shim YB (2006) Simultaneous analysis of nitrate and nitrite in a microfluidic device with a Cu-complex-modified electrode. *Electrophoresis* 27(22):4545–4554. <https://doi.org/10.1002/elps.200600240>
 56. Madasamy T, Pandiaraj M, Balamurugan M, Bhargava K, Sethy NK, Karunakaran C (2014) Copper, zinc superoxide dismutase and nitrate reductase coimmobilized bienzymatic biosensor for the simultaneous determination of nitrite and nitrate. *Biosens Bioelectron* 52:209–215. <https://doi.org/10.1016/j.bios.2013.08.036>